The International Journal Of Engineering And Science (IJES)
|| Volume || 5 || Issue || 4 || Pages || PP -49-56|| 2016 ||
ISSN (e): 2319 – 1813 ISSN (p): 2319 – 1805

Microstructural and Dielectric Characterization of Sr doped $Ba(Fe_{0.5}Ta_{0.5})O_3$ Ceramics

M.K.H Bhuiyan [1], M.A Gafur [2], M. N. I Khan[3], A. K. M. Akther Hossain[1]
[1)]*Department of Physics, Bangladesh University of Engineering and Technology, Dhaka 1000, Bangladesh*
[2)]*Pilot Plant & Process Development Centre, BCSIR, Dhaka-1205, Bangladesh*
[3)]*Materials Science Division, Atomic Energy Centre, Dhaka-1000, Bangladesh*

ABSTRACT
Solid state reaction method was used to synthesize $Ba_{1-x}Sr_x(Fe_{0.5}Ta_{0.5})O_3$ ceramic(x=0, 0.1, 0.2, 0.3, 0.4 and 0.5). The raw materials of making Sr doped $Ba(Fe_{0.5}Ta_{0.5})O_3$ were $BaCO_3$, $SrCO_3$, Fe_2O_3, Ta_2O_5 (purity better than 99%). Pellet and ring shaped samples prepared from each composition were sintered at 1400 and 1450ºC for 5 hour. The phase formation of $Ba_{1-x}Sr_x(Fe_{0.5}Ta_{0.5})O_3$ was checked using X-ray diffraction (XRD) technique and observed a cubic perovskite crystal structure in space group Pm3m (221). Microstructure of the individual compound was examined by the field emission scanning electron micrograph (FESEM). Grain size was found to be varied with Sr content. The lattice parameter decreased with increasing Sr content. Dielectric spectroscopy was applied to investigate the electrical properties of BSFT at room temperature and in a frequency range of 100Hz–100 MHz. An analysis of the dielectric constant ε′ and loss tangent tanδ with frequency was performed assuming a distribution of relaxation times. The low frequency dielectric dispersion corresponds to the DC electrical conductivity.
Keywords*: Ceramics, Dielectric, perovskite, space group, spectroscopy*

Date of Submission: 11 April 2016 Date of Accepted: 24 April 2016

I. Introduction

Ceramic materials are widely used for detectors, sensors, actuators, multilayer ceramic capacitor, computer memories, pyroelectric detectors, wireless communication systems, microelectronics, global positioning systems and other electronic devices [1]. This compounds having general formula ABO_3 show the perovskite structure. In the basic unit, the oxygen atoms form a cubic lattice of corner sharing octahedra with the B cations at their centers, while the A cations form a second inter penetrating cubic sub lattice located at 12 fold coordinated sites between octahedra [2]. Interestingly, most of the perovskite compounds that are of greatest technological interests are not simple systems but rather complex oxides with two different kinds of B-atoms such as $A(B'B'')O_3$. From a chemical point of view, two classes of compounds can be distinguished: homovalent and heterovalent compounds. Different kinds of B ion pairs show a variety of physical properties of perovskite [3]. Depending on the valences and the ionic radii, the B site cataions also settle either in an orderly or in a random fashion in the lattice [4]. In general in $BaTiO_3$ ceramics Fe^{3+} and Ta^{5+} are more stable than Ti^{4+}[5]. Z. Wang *et al* have reported a strong correlation between the dielectric properties and the mixed valent structure of Fe^{2+}/Fe^{3+} in Fe containing perovskite [6]. Thus in homovalent compounds, two B-atoms belong to the same column of the periodic table and the $A(B'_xB_{1-x}'')O_3$ compounds can thus have a composition x continuously ranging from 0 to 0.5

In the ceramic family Pb based materials have been most important because of their excellent piezoelectric properties and high curie points. Many researchers discover their sharp increases in the piezoelectric and relaxor behavior. Their phase transition also gradual and shows a broad peak [7]. But lead based oxides which are toxic and lead oxides evaporate easily causing the environmental pollution [8]. V. R Palker *et al*. have been successful in converting ferroelectric $PbTiO_3$ into magnetoelectric material by partially substituting Fe at Ti site [9]. The shift of the maximum value of dielectric constant versus temperature with the substitution of Ti with Fe and Ta in $BaTi_{1-x}Ta_{x/2}Fe_{x/2}O_3$ was reported by Goabiao*et al*. [10].

There is great technological demand if ferroelectricity and ferromagnetism coexist at room temperature. However, in reality, there is a scarcity of materials exhibiting both behavior at room temperature [11] possibly due to the fact that transition metal *d* electrons, which are essential for the presence of magnetic moment, reduce lattice distortion which is essential for ferroelectric behavior. Thus, additional structural or electronic driving force is required for ferroelectric and magnetic ordering to coexist. Although a certain number of materials with ferroelectricity and ferromagnetism exists, the coupling between those two properties is not always large enough [12-14].

Recently, Xin*et al*. have studied dielectric and magnetic properties of $Sr(Fe_{1/2}Ta_{1/2})O_3$ The nonlinear magnetic behavior is observed at 10 and 50 K [15]. The transition temperature of $BaFeO_3$, $SrFeO_3$ and $CaFeO_3$ were also reported to vary with their ionic radii by several authors [16-18] including Saha and Sinha [19], Intatha et al. [20], Fang et al [21], Reveski et al [22] Nedeclu et al [23], Tezuka et al [24].

Dielectric constant, dielectric loss, impedance are important tools for dielectric characterizations. These parameters are depended on the polarization, pores, grain, grain boundaries and their interfaces etc.Considering the above results it is necessary for understanding structural, dielectric magnetic aspects of Pb free ceramics. In the present study a systematic investigation of Sr substituted $Ba(Fe_{0.5}Ta_{0.5})O_3$ was performed.

II. Experimental details

2.1 Materials and method

Ceramic oxides $Ba_{1-x}Sr_x(Fe_{0.5}Ta_{0.5})O_3$, (where x = 0, 0.1, 0.2, 0.3,0.4 and 0.5) were prepared by a solid-state reaction technique. High-purity (~99.9%) ingredients: $BaCO_3$, $SrCO_3$, Fe_2O_3, Ta_2O_5 were used for the preparation of BSFT ceramics. These chemicals were taken in stoichiometric ratio, and mixed for 24 h. then the mixed powders were calcined in air at 1050°C for 5 h with a heating rate of 10ºC/min and cooling rate of 5ºC/min in a furnace to establish the course of nucleation for the grain growth and to felicitate the decomposition of the substituent oxides/carbonates. The calcined powder of above mentioned ceramics were regrinded and used to make pellet of diameter~ 12 mm and thickness ~1mm using polyvinyl alcohol as binder. The pellets were sintered at 1400 and 1450 °C for 5h and then brought to room temperature because the sintering process is key issue to develop the most appropriate structure for the application to complete the inter-diffusion of the component metal ions into the desired crystal lattice and to establish the appropriate valencies for the multi-valent ions.

2.2 Characterizations

The phase formation of all the BSFT ceramics were characterized by Philips Pan Analytic Xpert Pro X-ray diffractometer with Cu-Kα radiation (λ = 1.541Å) in a wide range of Braggs angles 2θ. The lattice parameters were calculated from XRD data. The microstructure of the compositions was analyzed using a Field emission scanning electron microscope (FESEM) (JEOL JSM 7600 F, Japan). The bulk density, ρ_B of each composition was calculated using the relation: $\rho_B=m/(\pi r^2 t)$, where *m* is the mass, *r* is the radius and *t* is the thickness of the pellet. The theoretical density, ρ_x were determined by the general formula, : $\rho_x=nM/N_AV$, where *n* is the number of atoms in a unit cell, *M* is the molar mass of the sample, N_A is the Avogadro's number and *V* is the volume of the unit cell. The porosity of the samples were calculated using the formula, $P(\%)=[\rho_x-\rho_B)/\rho_x]\times100\%$.

The frequency dependence of dielectric constant and dielectric loss were measured using Wayne Kerr Impedance Analyzer (B 6500 series) in the frequency range 100Hz-100MHz. For dielectric measurements all the samples were painted with conducting silver paste on both sides to ensure good electrical contacts. The dielectric constant, ε′ was calculated using the formula: $\varepsilon'=Cd/\varepsilon_0 A$, where *C* is the capacitance of pellet, *d* is the thickness, *A* is the cross-sectional area of the electrode and ε_0 is the permittivity in free space. The AC conductivity, σ_{AC}, of the samples was calculated using the relation: $\sigma AC=\omega\varepsilon_0\varepsilon'\tan\delta$, where ω is the angular frequency and $\tan\delta$ is the dielectric loss.

III. Results and discussion

3.1. X-ray diffraction analysis

X-ray diffraction (XRD) is a versatile, non-destructive technique that reveals the detailed information about the chemical composition and crystallographic structure of natural and manufactured materials. The Rietveld refinement for the XRD data was performed using the TOPAS-4.2 Software. The XRD pattern for the $Ba_{1-x}Sr_x(Fe_{0.5}Ta_{0.5})O_3$ sintered at 1400^{O}C and 1450^{O}C are shown in Fig. 1 and 2 respectively confirm a cubic crystal structure with space group P m3m (2 2 1). All the reflection peaks of the XRD pattern of the samples were indexed, and the lattice parameters were determined.

Firstly, the XRD patterns are virtually the same and show only single phase perovskite structure without the evidence of the second phase. It implies that Sr^{2+}ions have entered the unit cell maintaining the perovskite structure of solid solution. XRD patterns of $Ba(Fe_{0.5}Ta_{0.5})O_3$ and Sr doped BFT ceramics are in agreement with the respective joint committee on powder diffraction standards(JCPDS, PDF no. 01075-0426).

Secondly, the diffraction peaks of samples move to the lower angle side with the increase of Sr content. The systematic shift of the XRD peaks indicates the solid solubility of Sr in $Ba(Fe_{0.5}Ta_{0.5})O_3$ lattice and the decrease in lattice parameter with the increasing of Sr content. The Sr content effects the lattice parameters of $Ba_{1-x}Sr_x(Fe_{0.5}Ta_{0.5})O_3$ sintered at 1400^{O}C and 1450^{O}C ceramics . It can be explained by the substitution larger Sr^{2+} ions for Ba^{2+} ions on the A sites of the lattice. The ionic radius of Sr^{2+} (1.35Å) is smaller than that of Ba^{2+} (1.18Å).

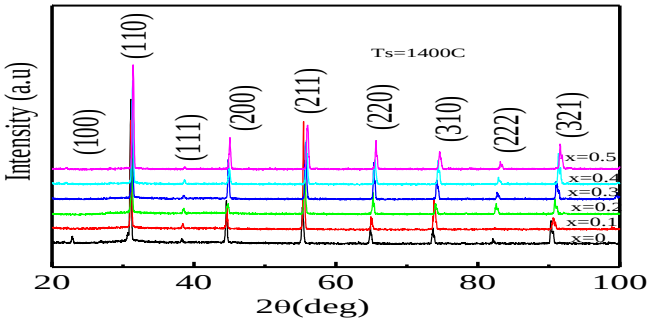

Figure 1: XRD Patterns of various $Ba_{1-x}Sr_x(Fe_{0.5}Ta_{0.5})O_3$ sintered at 1400°C

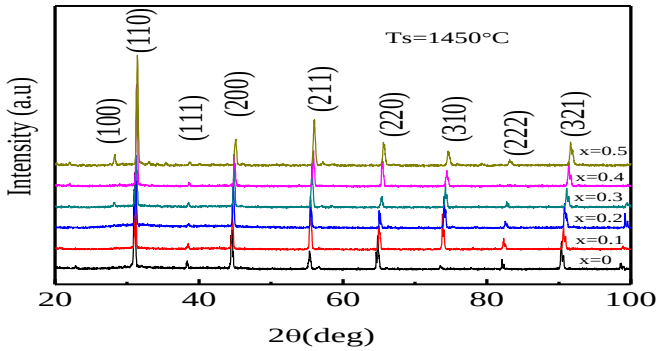

Figure 2: XRD Patterns of various $Ba_{1-x}Sr_x(Fe_{0.5}Ta_{0.5})O_3$ sintered at 1450°C

3.2 Surface morphology

Morphological analysis of grain and grain boundaries of the $Ba_{1-x}Sr_x(Fe_{0.5}Ta_{0.5})O_3$ ceramics was carried out with Field Emission Scanning Electron Microscope (FESEM).The grain size controls the properties of the ceramic materials. The average grain size has been calculated using the relation $\bar{D} = 1.56\bar{L}$ [25], where $\bar{D}$ is the average grain size and $\bar{L}$ is the average intercept length over a large number of grains as measured on the plane of the sample.

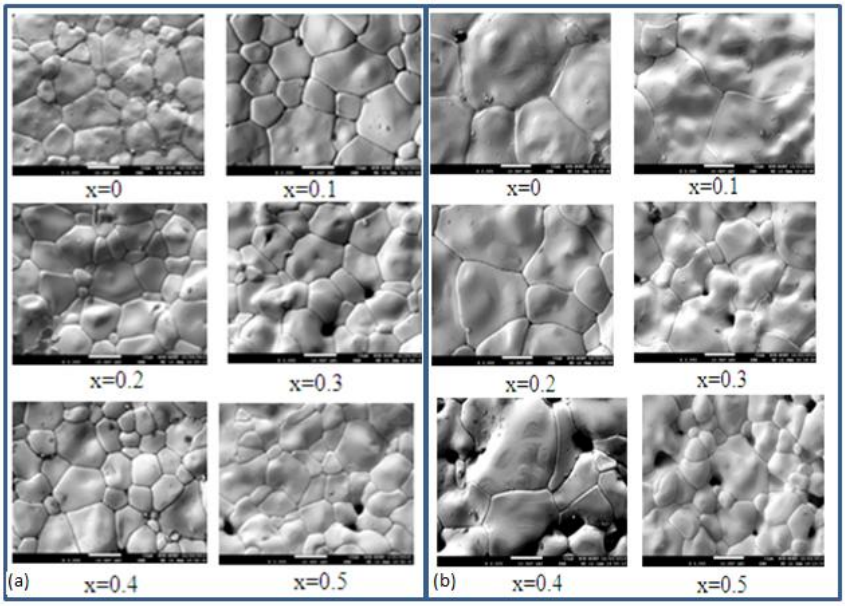

Figure 3: Typical SEM micrographs of the$Ba_{1-x}Sr_x(Fe_{0.5}Ta_{0.5})O_3$ x=0, x=0.1,x=0.2 x=0.3, x=0.4,x=0.5 sintered at (a) 1400 and (b) 1450°C respectively.

Figure 3 (a) and (b) shows the micro graph of the surface of the $Ba_{1-x}Sr_x(Fe_{0.5}Ta_{0.5})O_3$ samples sintered at 1400^0 and 1450^0C. From the figure it is observed that there is coexistence of small and large grain. Grain boundaries would be pinned by the defect, inhibiting grain growth and resulting in small grain. The average grain size varies from 11.49μm to 26 μm. For x=0.1 and in $Ba_{1-x}Sr_x(Fe_{0.5}Ta_{0.5})O_3$ ceramics the grain size increased as shown in figure 4. The grain size increases due to smaller grains nucleation as evidenced by the FESEM pictures and this considerable grain growth would release the internal stress field from the grain boundaries in order to enhance grains bonding. The growth mechanism occurs by the grain boundary motion due to a reduction of the total grain boundary surface energy. The thermal energy leads to an increase in the diffusion rate and consequently intensifies the formation of necks between the grains. The grain size decreases because the nucleation rate is greater than the growth rate and also the high mobility of ions but for another composition the grain size decreased for both sintering temperature. Grain size is strongly influence by the rate of nucleation and grain growth and temperature.

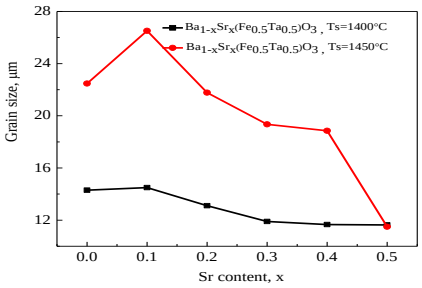

Figure 4: Variation of grain size on various $Ba_{1-x}Sr_x(Fe_{0.5}Ta_{0.5})O_3$ sintered at 1400 and 1450°C

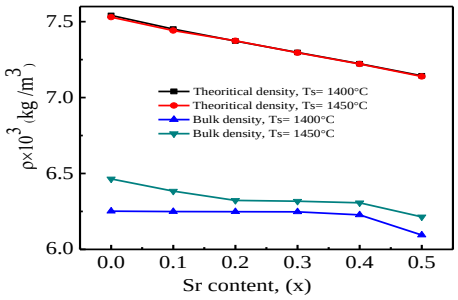

Figure 5: Variation of density on various $Ba_{1-x}Sr_x(Fe_{0.5}Ta_{0.5})O_3$ sintered at 1400 and 1450°C

Density and porosity play an important role in controlling the microstructure and the physical properties of the $Ba_{1-x}Sr_x(Fe_{0.5}Ta_{0.5})O_3$ ceramics. Figure 5 shows the bulk density of $Ba_{1-x}Sr_x(Fe_{0.5}Ta_{0.5})O_3$ ceramics sintered at 1400^0 and 1450^0C as a function of Sr content. It is observed that for $Ba_{1-x}Sr_x(Fe_{0.5}Ta_{0.5})O_3$ samples, sintered at 1400^0C, the bulk density increases and the corresponding porosity decreases for Sr content with the value of x=0.1 The bulk density decreases and the correspondingly porosity increases. The decrease of density with the increase of Sr content may be attributed to the fact the atomic weight and density of Sr content (87.616 gm/mol, 2.64gm/cm^3) is smaller than that of Ba(137.326 gm/mol, 3.52gm/cm^3)

3.3 Dielectric properties

Fig 6, 7 and 8, 9 represent the variation of the dielectric constant (ε′) and dielectric loss (tan δ) with frequency of $Ba_{1-x}Sr_x(Fe_{0.5}Ta_{0.5})O_3$ samples sintered at 1400 and 1450°C. It is observed that the value of ε′ for $Ba(Fe_{0.5}Ta_{0.5})O_3$ is higher as compared to the BSFT due to lower Sr concentration. It was confirm that Sr doped $Ba(Fe_{0.5}Ta_{0.5})O_3$ forms primarily according to an ionic, Fe and Ta vacancy compensation mechanism leading to general formula $Ba_{1-x}Sr_x(Fe_{0.5}Ta_{0.5})O_3$[26]. It is observed that the ε′ decreases with increasing the frequency for all compositions. The amount of oxygen loss in the Sr doped $Ba(Fe_{0.5}Ta_{0.5})O_3$ is very small and difficult to control specially heating in air> 1400 and 1450°C. The electric properties are very sensitive to oxygen nonstoichiometry, and room temperature resistance is heavily dependent on degree of reoxidation that occurs during cooling, on kinetic variables, such as cooling rate.

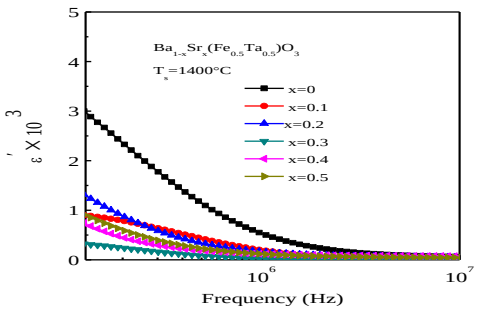

Figure 6: Variation of dielectric constant with frequency of various $Ba_{1-x}Sr_x(Fe_{0.5}Ta_{0.5})O_3$ sintered at 1400°C

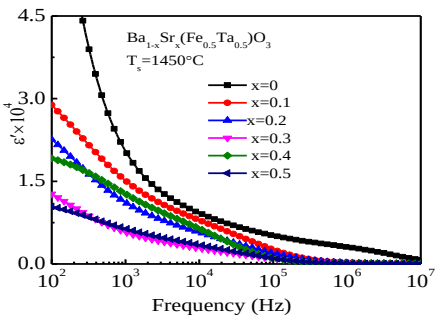

Figure 7: Variation of dielectric constant with frequency of various $Ba_{1-x}Sr_x(Fe_{0.5}Ta_{0.5})O_3$ sintered at 1450°C

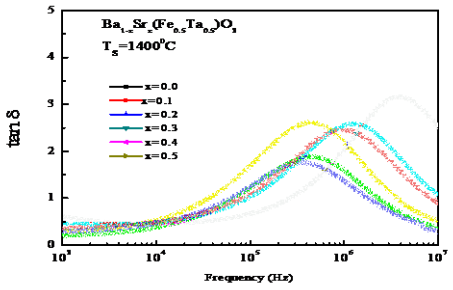

Figure 8: Variation of tan δ with log frequency of various $Ba_{1-x}Sr_x(Fe_{0.5}Ta_{0.5})O_3$ sintered at 1400°C

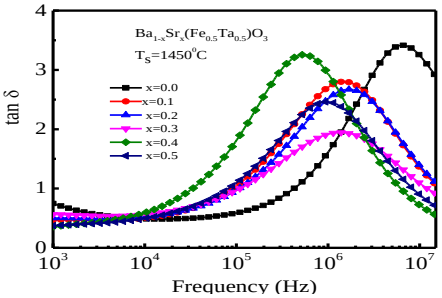

Figure 9: Variation of tan δ with log frequency of various $Ba_{1-x}Sr_x(Fe_{0.5}Ta_{0.5})O_3$ sintered at 1450°C

In general, there is a characteristic relaxation time for the charge transport and therefore the values of ε′ depend on the applied frequency. At high frequency region (> 0.1MHz), the values of ε′ become independent of frequency for all compositions. In the low frequency region, different types of polarizations such as dipolar, electronic, ionic and interfacial polarization are the main sources of dielectric constant [27]. With the increase of frequency beyond a certain limit, dipoles are not able to align themselves with the applied electric field and contribution from some of these polarizations cease except electronic polarization. Only electronic polarization has a significant contribution to the dielectric constant at higher frequencies. In electronic polarization, the electric dipoles are unable to follow the first alteration of the applied alternating electric field beyond certain critical frequency.

There is little variation in the value of ε′ which pertains to space charge polarization. The value of ε′ in synthesized samples is not usually intrinsic but rather associated with polarization and inhomogeneous dielectric structure. These inhomogneities are due to grain structure and pores. Also ε′ remain unchanged as the frequency increases. The variation of ε′ with composition could be attributed to the polarized space charge. It is basically due to the difference in radius of substituted ions. Due to the smaller ionic radius of Sr which is diffused well into the most of Ba sites and leaving vacancies for very few defects or voids for the generation of absorption current, which results in dielectric loss. In the low frequency range, dielectric loss is determined by the influence of ionic conductivity.

There might be a another reason for the maximum dielectric loss which may be attributed due to the fact that period of relaxation process is same as the period of applied field. In other words, when the relaxation time is large as compared to the period of the applied field, losses are small. Similarly, when relaxation process is rapid as compared to the frequency of the applied field, losses are small.

The higher values of ε′ at lower frequencies are due to the presence of all different types of polarizations (i.e., dipolar, atomic, ionic, electronic contribution) in the materials. At high frequencies, some of the above mentioned polarizations may have less contribution in ε′. The high value of ε′ in the low frequency region has been explained using Maxwell-Wagner (MW) polarization effect. Thus high values of permittivity are not usually intrinsic, but rather associated with heterogeneous conduction in the grain and grain boundary of the compounds. That is due to the grains of the sample are separated by more insulating inter grain barriers, in a boundary layer capacitor. All the samples show almost same behavior. Furthermore, tan δ was observed to increase with frequency and remains same even if the concentration of Sr changes in sample composition.

3.4 Impedance spectra analysis

Figure 10, 11 and 12 and 13 show the variations in real and imaginary part (Z') of impedance with frequency sintered at 1400 and 1450°C. It is observed that the magnitude of Z' gradually decreases with increasing frequency. The decrease in Z' indicates that the conduction is increasing with frequency. It becomes almost frequency independent. The higher values of Z' at lower frequencies means the polarization in the compositions is larger.

For a BSFT samples having interfacial boundary layers (grain-boundary), may be obtained in the complex plane plot, which can be explained as two parallel RC elements connected in series: one branch is associated with the grain and other with the grain-boundary of the sample. The merger of Z' at higher frequencies indicates possible release of space charge polarization/accumulation at the boundaries of homogeneous phases in the compositions under the applied external field [28, 29]. On the other hand with the increase of Sr concentration, the values of Z' decrease in the low frequency ranges (up to a certain frequency).

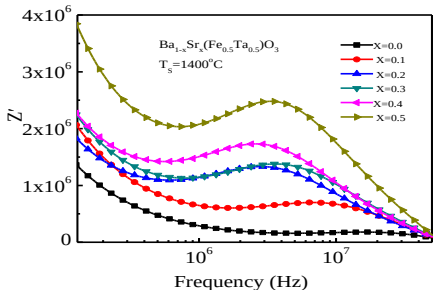

Figure 10: Variation of real part of impedance with frequency of $Ba_{1-x}Sr_x(Fe_{0.5}Ta_{0.5})O_3$ sintered at 1400°C

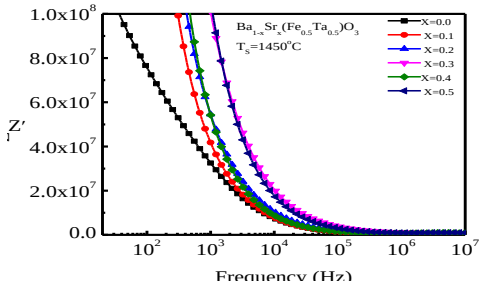

Figure 11: Variation of real part of impedance with frequency of $Ba_{1-x}Sr_x(Fe_{0.5}Ta_{0.5})O_3$ sintered at 1450°C

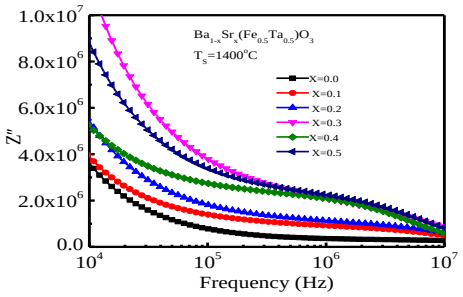

Figure 12: Variation of imaginary part of impedance with frequency of $Ba_{1-x}Sr_x(Fe_{0.5}Ta_{0.5})O_3$ sintered at 1400°C

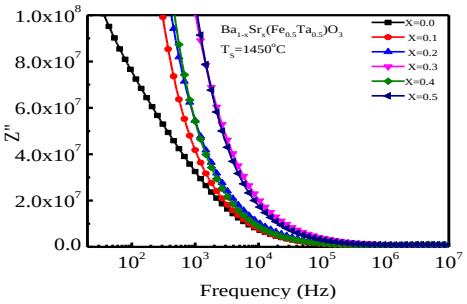

Figure 13: Variation of imaginary part of impedance with frequency of $Ba_{1-x}Sr_x(Fe_{0.5}Ta_{0.5})O_3$ sintered at 1450°C

The grain boundary impedance is out of the measurement scale, suggesting the insulating behavior of the samples. The complex impedance spectra exhibit the single semicircular arcs, it can be said that the electrodes and contacts do not have significant impedance because electrode-contact would result in an additional semicircle. A single semicircle indicates that only one primary mechanism is responsible for the electrical conduction within the sample. In other words, the absence of other semicircles in the complex impedance plots suggests the dominance of bulk contributions in the compositions. Cole-Cole for the compositions with T_s= 1400 and 1450ºC have been showed in fig. 14 and 15, respectively. The expressions from fig.16 suggest that plotting gives a semicircle for a conducting Debye material, which is similar to the dielectric spectrum presented in the Cole-Cole plot of a pure Debye response without dc conductivity.

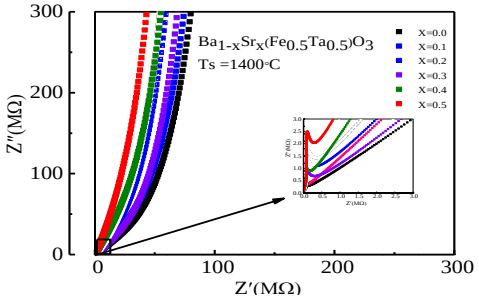

Figure 14: Cole-Cole plot of complex impedance spectra of various $Ba_{1-x}Sr_x(Fe_{0.5}Ta_{0.5})O_3$ sintered at 1400°C

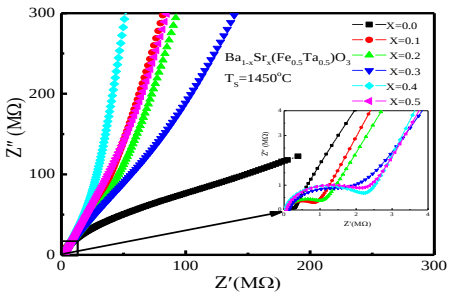

Figure 15 : Cole-Cole plot of complex impedance spectra of various $Ba_{1-x}Sr_x(Fe_{0.5}Ta_{0.5})O_3$ sintered at 1450°C

3.5 AC conductivity

Figure 16 and 17 shows the variation of AC conductivity (σ_{AC}) with frequency for BSFT samples sintered at 1400 and 1450°C. It is observed that the increase of conductivity is less at low frequency, but it is rapid at high frequency. The increase of σ_{AC} with Sr concentration is due to the generation of the charge carrier concentration [30]. Furthermore, the increase of σ_{AC} with frequency is generally attributed to the dipole polarization, i.e., the rotation of diploes between two equilibrium positions is involved. It is the spontaneous alignment of dipoles in one of the equilibrium positions that give rise to the nonlinear polarization behavior of this composition. In low frequency region, the conductivity is almost independent of frequency which

corresponds to DC conductivity (σ_{DC}) because the resistive grain boundaries are more active at low frequencies according to the Maxwell-Wagner double layer model for dielectrics. On the other hand, in the high frequency region which is known as hopping region, AC conductivity increases [31] because at higher frequencies the conductive grains become more active thereby increasing hopping of charge carriers [32] and obeys the following Joncher's law: $\sigma_{AC}(\omega)=\sigma_0+A\omega^s$, where $\sigma_{AC}(\omega)$ is the total electrical conductivity, σ_0 is the frequency-independent dc conductivity, where A is a pre-exponential factor, which is temperature-dependent, [33] and *s* is the power law exponent. The exponent *s* represents the degree of interaction between mobile ions with the lattice around them. The pre factor *A* determines the strength of polarizability.

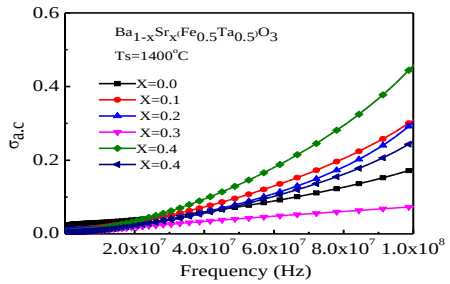

Figure 16: Variation of AC conductivity (σ_{AC}) with frequency of $Ba_{1-x}Sr_x(Fe_{0.5}Ta_{0.5})O_3$ sintered at 1400°C

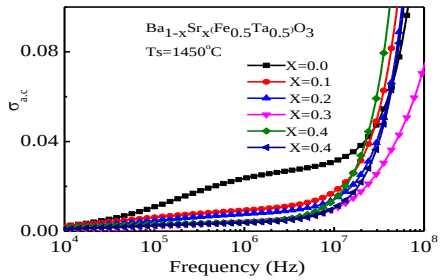

Figure 17: Variation of AC conductivity (σ_{AC}) with frequency of $Ba_{1-x}Sr_x(Fe_{0.5}Ta_{0.5})O_3$ sintered at 1450°C

In small polaron hopping, ac conductivity increases with frequency whereas in large polaron hopping ac conductivity decreases with frequency [34].The electrical conduction mechanism in terms of the electron and polaron hopping model. It is evident that the conductivity increases with the increase of frequency for all compositions and plots are linear which indicates the conduction in these compositions is due to small polarons associated with lattice strain accompanied by free charges. The grain boundaries are more active and the role of polaron hopping process is minor when the frequency of the applied field is low. On the contrary, when the frequency of the applied field increases, the conductive phase becomes more active and thereby increasing the importance of small polaron hopping conduction. Therefore a gradual increase in conductivity was observed with frequency. The lower and higher frequency regions represent the nondiffusing and localized diffusing modes, respectively, and based on this theory Ishii *et al.* [35].

IV. Conclusions

BSFT Ceramics were successfully synthesized using the conventional solid state reaction. X-ray diffraction patterns confirms a cubic crystal structure with space group P m3m (2 2 1).The frequency dependent dielectric properties show the usual dielectric dispersion behavior for all the compositions which can be explained on the basis of Maxwell-Wagner interfacial polarization effect. At higher frequencies, the dielectric constant remains independent of frequency because electric dipoles with large relaxation time cease to respond.

The dielectric loss decreases at higher frequencies due to the suppression of domain wall motion. It is observed that the composites have both the grain and grain boundary effects to the electrical properties. The σ_{AC} increases with increasing frequency showing small polaron hopping type of conduction phenomenon in these compositions. The ac electrical conductivity increases with increasing frequency which is generally attributed to the presence of space charge. Thus, in the low frequency region the conductivity is almost constant. In the high frequency region, where the conductivity increases strongly with frequency, the transport phenomena are dominated by contribution from hopping mechanism.

Acknowledgements

This work is supported by the CASR of Bangladesh University of Engineering and Technology (BUET).

References

[1] S. Mandolappa, R.Sagar, N.Sharanappa and R. L Raibagkar, Ceram. Bull. Mater. Sci.36. 4. (2013) 601-606
[2] A. Dutta, C. Bharti, T.P. Sinha, Mater. Research Bull. 43. (2008) 1246-1254
[3] Z.Wang and X. Ming Chen, Journal of physics D: Appl. Phys. 42.(2009) 175005(1-5)
[4] Z.Wang Z, X. M Chen, Ni L, Y .Y Liu and X Q Appl. Phys. Lett. 90.(2007)102905.
[5] X.G. Tang, H.L.W. Chan and A.L. Ding,Thin Solid. Film. 460, (2004) 227-231
[6] Z. Wang, X. M Chen, L. Ni and X.Q Liu Appl. Phys. Lett. 90 (2007) 022904.
[8] L. Zhang,S. Wang,X.Wang, and K.Huanga,ECS J. Solid State Science and Technology, 1 (2).(2012)2162, N29-N32
[9] V.R Palkar, S.K and Malik, Solid. State. Commun.134.(2005) 783-786
[10] L.Guobao,S.Liu,FuhuiLiao, S.Tian,X. Jing, J.Lin,Y. Uesu, K.Kohn,K. Saitoh, M.Terauchi,NailiDi, and Z.Cheng , J. Solid. State. Chemistry 177, (2004) 1695-1703
[11] F. A. Somlenskii, , I.Chupis , and E., Ferroelectromagnet, Soviet Physics Uspekhi, 25. (1982). 475-493

[12] M.Kumar, and K. L Yadav, Appl. Phys.Lett. 91. 242901.(2007) 1-3
[13] N. A Hill, The J.Phys.Chem.B.104.(2000)6694-6709
[14] D. I Khomskii, J.Magn. Magn.Mater.306. (2006)1-8
[15] L. Xin, X. Qiang Liu, H. Jian Zhao, W. Zhi Yang and X. Ming Chen, "J. Am.Ceram.Soc.96.No. 4. (2013).1188-1192
[16] C. Callender, D. P. Norton , R.Das, Hebard, J. A. F. Budai, D. Appl.Phys.Lett. 92.(2008)012514(1-3)
[17] Z. Ali, I. Ahmad, B. Khan, I. Khan, Chinsese .Phys, Lett.30. (2013) 047504(1-5)
[18] N. Hayashi, T. Yamamoto, H. Kageyyama, M. Nish,Yoshikata, Wantabe , T. Kawakami ,Y. Matsushita, A. Fujimori and M.Takano, Angewandte Chemie.Int. Ed. 50.(2011).12547-12550.
[19] S. Saha and T. P. Sinha. *J. Phys.Condens. Mat.*14.(2002) 249-258
[20] U. Intatha, S. Eitssayeam, J. Wang and T. Tunkasiri. *Curr. Appl.Physic*. 10.(2010) 21-25
[21] B. Fang, Z. Cheng, R. Sun and C. Ding. *J. Alloy. Comp*..471.(2009) 539-543
[22] I.P. Raevski, S. A. Prosandeev, A. S. Bogatin, M. A.Malitskaya and L. Jastrabik. *J. Appl.Phys*. 93.(2003).4130-4136
[23] L. Nedelcu, M. I. Toacsan, M. G. Banciu and A. Ioachim. *J.Alloy. Compd*. 509.(2011) 477-481
[24] K.Tezuka, K. Henimi, Y. Hinatsu, N. M. Masaki.*J. Solid.State.Chem*..154. (2000)591-597
[25] M.I. Mendelson, J. Am. Ceram. Soc. 52 (1969) 443-446
[26] D. Finlay, Morrison, C. Derek ,Sinclair, and R. West Anthony *J. Am. Ceram. Soc*.,**84**[3] 5(2001), 31-38
[27] A. Sharma, R.K. Kotnala, N.S. Negi, J. Alloys Compd. 582 (2014) 628-634
[28] B. Behera, P. Nayak, R.N.P. Choudhary, Cent. Eur. J. Phys. 6 (2008) 289-295
[29] J. Plocharski, W. Wieczoreck, Solid State Ion. 28-30.(1988) 979-982
[30] S. Panteny, C.R. Bowen, R. Stevens, J. Mater. Sci. 41 (2006) 3845-3851
[31] O. Bidault, P. Goux, M. Kchikech, M. Belkaoumi, M. Maglione, Phys. Rev. B. 49 (1994) 7868-7873
[32] I.G. Austin, N.F. Mott, Adv. Phys. 18(1969) 41.
[33] A. K. Jonscher, Nature. 267.(1977) 673-679
[34] M.S. Khandekar, R.C. Kambale, J.Y. Patil, Y.D. Kolekar, S.S. Suryavanshi, J. Alloys Compd. 509.(2011) 1861-1865
[35] T. Ishii, T. Abe, H. Shirai, Solid State Commun. 127.(2003) 737-741